CHAPTER 15: PARALLELS BETWEEN MAIN GROUP AND ORGANOMETALLIC CHEMISTRY

15.1 **a.** $Mn_2(CO)_{10} + Br_2 \longrightarrow 2\ Mn(CO)_5Br$

b. $HCCl_3 + \text{excess}[Co(CO)_4]^- \longrightarrow$

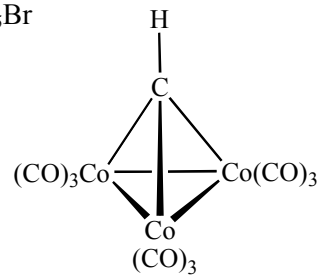

c. $Co_2(CO)_8 + (SCN)_2 \longrightarrow 2\ NCSCo(CO)_4$

d. $Co_2(CO)_8 + C_6H_5–C{\equiv}C–C_6H_5 \longrightarrow$

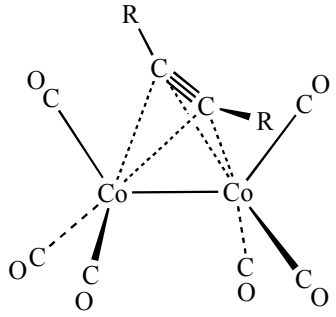

e. $Mn_2(CO)_{10} + [(\eta^5\text{-}C_5H_5)Fe(CO)_2]_2 \longrightarrow 2\ (CO)_5Mn–Fe(\eta^5\text{-}C_5H_5)(CO)_2$

15.2 **a.** $Tc(CO)_5 \leftarrow O \rightarrow CH_3$

b. $[Re(CO)_4]^- \leftarrow O \rightarrow CH_2$

c. $[Co(CN)_5]^{3-} \leftarrow O \rightarrow CH_3$

d. $[CpFe(C_6H_5)]^+ \leftarrow O \rightarrow CH_4$

e. $[Mn(CO)_5]^+ \leftarrow O \rightarrow CH_3^+$

f. $Os_2(CO)_8 \leftarrow O \rightarrow H_2C{=}CH_2$

15.3 Many examples are possible. Two for each:

a. $CH_3 \leftarrow O \rightarrow (\eta^6\text{-}C_6H_6)Mn(PPh_3)_2$
$CH_3 \leftarrow O \rightarrow [Ni(CS)(PMe_3)_2Cl_2]^+$

b. $CH \leftarrow O \rightarrow (\eta^4\text{-}C_4H_4)Co(CS)$
$CH \leftarrow O \rightarrow (\eta^6\text{-}C_6H_6)Rh$

c. $CH_3^+ \leftarrow\!\!\!\!\!\!\rightarrow Mo(borazine)(PMe_3)(CS)$
$CH_3^+ \leftarrow\!\!\!\!\!\!\rightarrow [V(CO)_3(en)]^-$

d. $CH_3^- \leftarrow\!\!\!\!\!\!\rightarrow (\eta^8\text{-}C_8H_8)Ru(PEt_3)$
$CH_3^- \leftarrow\!\!\!\!\!\!\rightarrow [Co(N_2)(CO)_2(bipy)]^+$

e. $(\eta^5\text{-}C_5H_5)Fe(CO)_2 \leftarrow\!\!\!\!\!\!\rightarrow Co(CO)_3Cl_2$
$(\eta^5\text{-}C_5H_5)Fe(CO)_2 \leftarrow\!\!\!\!\!\!\rightarrow [(\eta^6\text{-}C_6H_6)Cr(CO)_2]^-$

f. $Sn(CH_3)_2 \leftarrow\!\!\!\!\!\!\rightarrow (\eta^5\text{-}C_5H_5)Ir(CO)$
$Sn(CH_3)_2 \leftarrow\!\!\!\!\!\!\rightarrow [Tc(CO)_4]^-$

15.4 Many possibilities exist; some of those given here may not be synthetically accessible.

a. $C_2H_4 \leftarrow\!\!\!\!\!\!\rightarrow (CO)_4Fe{=}Fe(CO)_4$

b. $P_4 \leftarrow\!\!\!\!\!\!\rightarrow [Ir(CO)_3]_4$

c. *cyclo*-$C_4H_8 \leftarrow\!\!\!\!\!\!\rightarrow$ 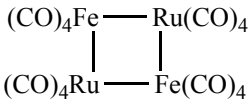

d. $S_8 \leftarrow\!\!\!\!\!\!\rightarrow$ *cyclo*-$[Fe(CO)_4]_8$

15.5 **a.** All three complexes are 18 electron species, with the benzene ring of $[(C_5Me_5)Fe(C_6H_6)]^+$ replaced by three carbonyl groups or two carbonyls and a phosphine. All have a formal coordination number of six.

b. The experimental results are more complex than might be expected.

$[(C_5Me_5)Fe(C_6H_5)]^+ + H^-$ → 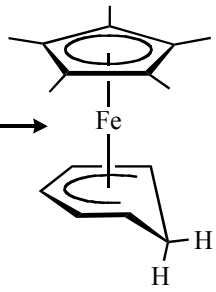

$[(\eta^5\text{-}C_5H_5)Fe(CO)_3]^+ + H^- \longrightarrow (\eta^5\text{-}C_5H_5)Fe(CO)_2H \longrightarrow [(\eta^5\text{-}C_5H_5)Fe(CO)_2]_2 + H_2$

$[(\eta^5\text{-}C_5H_5)Fe(CO)_2PPh_3]^+ + H^- \longrightarrow$ 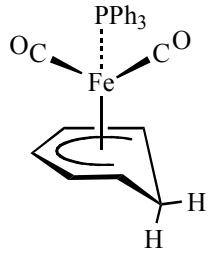

(See A. Davison, M. L. H. Green, and G. Wilkinson, *J. Chem. Soc.*, **1961**, 3172.)

15.6 **a.** CH_2, $Fe(CO)_4$, $[Mn(CO)_4]^-$, and PR_2 each has two frontier orbitals, each with one electron. Each fragment is two ligands short of the parent polyhedron (octahedron or tetrahedron).

b. $Fe(CO)_4$ and CpRh(CO) each has two frontier orbitals, each with one electron.

c. $[Re(CO)_4]^-$ has two frontier orbitals, with one electron in each. R_2C is isolobal with two frontier orbitals, each with one electron.

15.7 The $W(Cp)(CO)_2$ fragments are isolobal with CR and CPh, each with three orbitals containing one electron each; PtR_2 and $Cu(C_5Me_5)$ are isolobal, each with two orbitals containing one electron each.

15.8 **a.** If Mn has the lower energy orbital, then the bonding molecular orbital has a greater contribution by the Mn orbital, and the electrons in the orbital are polarized toward Mn.

b. The gold orbitals are higher in energy. Rather than matching energies with the lowest of the π orbitals of the Cp ring, the Au orbitals will match better with the higher π orbitals, which have a nodal plane cutting across the ring.

15.9 **a.** CH_2 and $Fe(CO)_4$ are isolobal, each with two orbitals containing one electron apiece.

b. $Mn(CO)_2(C_5Me_5)$ is isolobal with $[Mn(CO)_5]^+$, a 16 electron species, which is in turn isolobal with CH_2. The Mn–Sn–Mo fragment is similar to allene, C=C=C, in which the double bonds force a linear geometry.

15.10 $[C(AuPPh_3)_5]^+$ Structure: slightly distorted trigonal bipyramid, as expected from VSEPR.

$[C(AuPPh_3)_6]^{2+}$ Structure: slightly distorted octahedron, as expected from VSEPR.

The structure of the 7-coordinate $[C(AuPPh_3)_7]^{3+}$ has not been reported, but interest in the realm of highly coordinated carbon compounds continues; for a recent update, see H. G. Raubenheimer and H. Schmidbaur, *Organometallics*, **2012**, *31*, 2507.

In these complexes, each of the $AuPPh_3$ groups can be viewed as having an *sp* hybrid orbital pointing in toward the carbon. Interactions between these hybrids with the *s* and *p* orbitals of carbon give rise to four bonding orbitals in each case. The eight valence electrons available fill these orbitals. The result is the equivalent of four bonds spread over the complex (bond order of 4/5 in $[C(AuPPh_3)_5]^+$ and 4/6 in $[C(AuPPh_3)_6]^{2+}$. Metal-metal bonding is also likely to contribute to the stability of these structures.

For more details, see H. Schmidbaur, et. al., *Angew. Chem. Int. Ed. Engl.*, **1989**, *28*, 463 and *Angew. Chem. Int. Ed. Engl.*, **1988**, *27*, 1544.

15.11 Carbonyl ligands are significantly stronger π acceptors than cyclopentadienyl. Replacing three CO ligands with Cp on each metal atom, therefore, leaves the metals with greater electron density for involvement in metal–metal bonding, leading to shorter metal–metal bonds in the cobalt complexes. In addition, there is a general decrease in atomic radii from left to right in this row of transition metals, so Co atoms are slightly smaller than Fe atoms (see Table 2.8).

15.12 **a.** The orbital interactions are similar in the two cases, except that the π orbitals of the P_5 ring are lower in energy than those of the C_5H_5 ring, resulting in a stronger ability of the P_5 ring to accept electrons from the metal (see also reference 11 in this chapter).

b. Because the P_5 ring acts as a strong acceptor, electrons are accepted into antibonding orbitals in the titanium complexes, leading to longer P–P distances than in P_5^- (calculated at 2.12 Å). The Ti–P distances are calculated to be shorter in the theoretical structure $[Ti(P_5)]^-$ than in $[Ti(P_5)_2]^{2-}$, in which ligands compete for electrons in the same *d* orbitals on the metal. The consequence is that the predicted P–P distance is longer (2.24 Å) in $[Ti(P_5)]^-$, where the ligand can act as a stronger acceptor because it is closer to the metal, than in $[Ti(P_5)_2]^{2-}$ (calculated: 2.175 Å; experimental in reference 11: 2.154 Å).

15.13 **a.** The $Mn(CO)_5$ fragments have a single electron in their HOMO, largely derived from the d_{z^2} (hybridized with the p_z orbital) of Mn. Lobes of the HOMOs of two $Mn(CO)_5$ fragments interact in a sigma fashion with the σ_g orbital of C_2 (see Figure 5.5 for the approximate shape) derived primarily from the p_z orbitals of the C atoms:

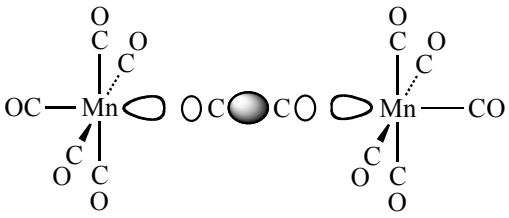

b. The empty π* orbitals of C_2 can interact with occupied *d* orbitals of $Mn(CO)_5$ fragments:

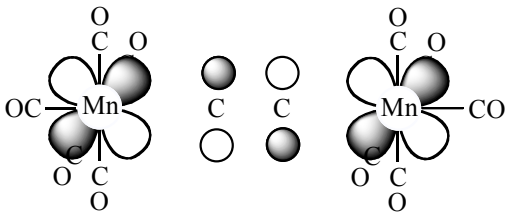

c. The reference points out other interactions, such as between π (bonding) orbitals of C_2 and $Mn(CO)_5$, and discusses the relative energies of the molecular orbitals of this molecule and other molecules having bridging C_2 ligands.

15.14 A staggered configuration is more likely, as predicted by VSEPR. The bonding is similar to that in the triply bonded $[Os_2Cl_8]^{2-}$.

15.15

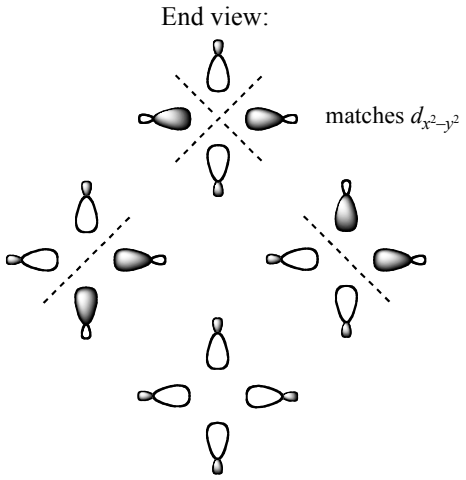

15.16 Cotton's explanation is that removal of an electron effectively changes the oxidation number of Tc, causing the *d* orbitals in $[TcCl_8]^{2-}$ to be smaller than those of $[TcCl_8]^{3-}$. This reduces the orbital overlap, weakening the bonding in spite of the higher formal bond order. The change is small—about 3 pm. (See F. A. Cotton and G. Wilkinson, *Advanced Inorganic Chemistry*, 5th Ed., Wiley, 1988. p. 1090.)

15.17 As the reference describes, these ions are isostructural and are based on octahedra fused at one mutual face (occupied by three bridging chlorine atoms). The shortening of the Re–Re distance upon reduction is attributed chiefly to two factors. As the complex is reduced, the net positive charge on each metal is reduced (the oxidation state changes from 4 to 3.5), which reduces the metal-metal repulsion. In addition, with the reduction of the metals, the metal *d* orbitals expand, enabling more effective overlap and stronger bonding.

15.18 This example is similar to the one presented in Figure 15.10. In compound **1** there are six DTolF ligands, each with a charge of 1–. Adding the charges of the bridging hydroxides, the total charge of the ligands in this complex is 8–. Consequently, the total charge on the Mo atoms must be 8+, or a charge of 4+ per Mo_2 unit. Each Mo^{2+} has 4 *d* electrons, giving 8 *d* electrons per Mo_2. Mo_2^{4+}, with its 8 *d* electrons, has an Mo–Mo bond order of 4 (Figure 15.10).

In compound **2** there are also six DTolF ligands. The bridging O^{2-} ligands result in a total ligand charge of 10–; consequently, the four molybdenums must carry an average charge of 2.5+, or 5+ per Mo_2 unit. There are now just 7 *d* electrons per Mo_2. From Figure 15.10 we can see that Mo_2^{5+}, with 7 *d* electrons, corresponds to a bond order of 3.5. The lower Mo–Mo bond order in **2** results in a longer bond.

15.19 **a.** Because the diphenylforamidinate ion has a charge of 1–, the iron atoms have an average oxidation state of 1.5, alternatively viewed as mixed-valent Fe(I) and Fe(II).

b. The iron atoms have a total of 7 [Fe(I)] + 6 [Fe(II)] = 13 *d* electrons. The 3*d* orbitals interact in sigma (d_{z^2}), pi (d_{xz} and d_{yz}), and delta (d_{xy} and $d_{x^2-y^2}$) fashions to generate bonding and antibonding orbitals of these types. The calculated order of energy of these orbitals is shown below. Experimental data and supporting calculations suggest that the singly occupied π*, σ*, δ, and δ* orbitals are very close in energy, favoring a high-spin arrangement that, in accordance with Hund's rule, results in seven electrons with parallel spin.

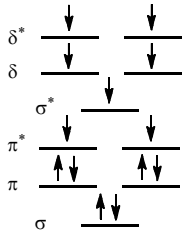

15.20 The clamping of the nitrogen atoms that bridge the chromium atoms is postulated to enforce short chromium—chromium bonds. The ligand, in effect, assists in pushing the chromium atoms together. Ligand design is critical to minimize inter-ligand substituent repulsion to maximize ligand chelation ability. While Figure 1 of the reference emphasizes steric effects, it is stated that repulsion between filled nitrogen and chromium nonbonding orbitals is maximized (resulting in further metal—metal bond contraction) when chelation is more robust. The aminopyridinates are shown in the same figure to chelate less effectively to the chromium atoms; the nitrogen substituents of the two ligands are directed slightly towards each other, reducing the efficacy of the chelate, and leading to longer chromium—chromium distances. The amidate substituents are directed away from the chromium—chromium bond, resulting in less inter-ligand repulsion, and slightly shorter chromium—chromium bonds. The guanidinates tune the clamping effect further by introducing steric pressure provided by the substituents emerging from the central carbon atom of the chelating ligand. This steric hindrance pushes the substituents of the chelating nitrogen atoms slightly towards the chromium atoms, resulting in the chromium atoms being pushed closer together.

The magnetic susceptibility results indicate that the dichromium complex **3** (see reference) features a singlet ground state, with no unpaired electrons. If the chromium atoms are both d^5 centers, then these 10 metal valence electrons will fill all five bonding molecular orbitals of the energy level diagram in Figure 15.9 to afford a quintuple bond.

15.21 It is proposed that $CH_3C \equiv CCH_3$ reacts with the quintuply bonded dichromium complex in a manner consistent with 2+2 cycloaddition resulting in a dichromium metallacycle with a carbon—carbon double bond and a chromium—chromium quadruple bond. The crystallographic data support this hypothesis on the basis of a carbon—carbon distance (132.6 pm) similar to that of ethylene (133.9 pm), and a chromium—chromium distance (192.5 pm) longer than that in the starting quintuply bonded complex (180.3 pm), consistent with a fourfold chromium—chromium bond order. Calculated bond orders (via DFT calculations) for the dichromium metallacyle product are 3.43 and 1.98 for the chromium—chromium and carbon—carbon bonds, respectively.

15.22 **a.**

O_h	E	$8C_3$	$6C_2$	$6C_4$	$3C_2$	i	$6S_4$	$6S_6$	$3\sigma_h$	$6\sigma_d$	
Γ (s, p_z)	6	0	0	2	2	0	0	0	4	2	
A_{1g}	1	1	1	1	1	1	1	1	1	1	
T_{1u}	3	0	–1	1	–1	–3	–1	0	1	1	
E_g	2	–1	0	0	2	2	0	–1	2	0	

Γ fits either the s or the p_z orbitals.

b. It can be seen from the table above that $\Gamma = A_{1g} + T_{1u} + E_g$. This can also be worked out by the more elaborate methods used in Chapter 4.

c. The reducible representation for the p_x and p_y orbitals and its components are shown in the following table. Figure 15.13 shows the three T_{1u} and the three T_{2g} group orbitals required (which also include some p_z contribution from two of the boron atoms). The T_{1g} and T_{2u} representations are for antibonding orbitals.

O_h	E	$8C_3$	$6C_2$	$6C_4$	$3C_2$	i	$6S_4$	$6S_6$	$3\sigma_h$	$6\sigma_d$	
$\Gamma_{x,y}$	12	0	0	0	–4	0	0	0	0	0	
T_{1g}	3	0	–1	1	–1	3	1	0	–1	–1	(R_x, R_y, R_z)
T_{1u}	3	0	–1	1	–1	–3	–1	0	1	1	(x, y, z)
T_{2g}	3	0	1	–1	–1	3	–1	0	–1	1	
T_{2u}	3	0	1	–1	–1	–3	1	0	1	–1	

15.23 The number of orbitals of each type can be obtained by analogy with the results for $B_6H_6^{2-}$ (Section 15.4.1):

2 valence atomic orbitals of B combine to form:
- 15 bonding orbitals ($2n + 1$) consisting of:
  - 8 framework MOs ($n + 1$)
    - 1 bonding orbital from overlap of *sp* orbitals
    - 7 bonding orbitals from overlap of *p* orbitals of B with *sp* hybrid orbitals or *p* orbitals of other B atoms
  - 7 B–H bonding orbitals (n)
- 13 nonbonding or antibonding orbitals

15.24 **a.** $C_2B_3H_7 \rightarrow B_5H_9 \rightarrow B_5H_5^{4-}$ *nido*

b. $B_6H_{12} \rightarrow B_6H_6^{6-}$ *arachno*

c. $B_{11}H_{11}^{2-}$ *closo*

d. $C_3B_5H_7 \rightarrow B_8H_{10} \rightarrow B_8H_8^{2-}$ *closo*

e. $CB_{10}H_{13}^{-} \rightarrow B_{11}H_{14}^{-} \rightarrow B_{11}H_{11}^{4-}$ *nido*

f. $B_{10}H_{14}^{2-} \rightarrow B_{10}H_{10}^{6-}$ *arachno*

15.25 **a.** $SB_{10}H_{10}^{2-} \rightarrow B_{11}H_{13}^{2-} \rightarrow B_{11}H_{11}^{4-}$ *nido*

b. $NCB_{10}H_{11} \rightarrow B_{12}H_{14} \rightarrow B_{12}H_{12}^{2-}$ *closo*

c. $SiC_2B_4H_{10} \rightarrow B_7H_{13} \rightarrow B_7H_7^{6-}$ *arachno*

d. $As_2C_2B_7H_9 \rightarrow B_{11}H_{15} \rightarrow B_{11}H_{11}^{4-}$ *nido*

e. $PCB_9H_{11}^{-} \rightarrow B_{11}H_{14}^{-} \rightarrow B_{11}H_{11}^{4-}$ *nido*

15.26 **a.** $B_3H_8(Mn(CO)_3) \rightarrow B_4H_8 \rightarrow B_4H_4^{4-}$ *nido*

b. $B_4H_6(CoCp)_2 \rightarrow B_6H_8 \rightarrow B_6H_6^{2-}$ *closo*

c. $C_2B_7H_{11}CoCp \rightarrow B_9H_{13}CoCp \rightarrow B_{10}H_{14} \rightarrow B_{10}H_{10}^{4-}$ *nido*

d. $B_5H_{10}FeCp \rightarrow B_6H_{10} \rightarrow B_6H_6^{4-}$ *nido*

e. $C_2B_9H_{11}Ru(CO)_3 \rightarrow B_{11}H_{13}Ru(CO)_3 \rightarrow B_{12}H_{14} \rightarrow B_{12}H_{12}^{2-}$ *closo*

15.27 **a.** $Ni(CO)_4$: CH_4 $Ni(CO)_2$: CH_2^{2+}
$Ni(CO)_3$: CH_3^{+} $Ni(CO)$: CH^{3+}

b. $[Bi_3Ni_4(CO)_6]^x$ The cluster needs $4n + 2 = 4(7) + 2 = 30$ cluster valence electrons for a *closo* classification (there are 7 Bi and Ni atoms in the core of the cluster). Each Bi atom contributes its 5 valence electrons, and each CO ligand contributes 2, for a total of 3(5) + 6(2) =27. Three additional electrons are needed for a total of 30; consequently, the charge must be $\boldsymbol{x = 3-}$; the formula is $[Bi_3Ni_4(CO)_6]^{3-}$. (See reference and citations therein for additional details on electron counting.)

c. $[Bi_xNi_4(CO)_6]^{2-}$ The cluster valence count starts with 6 CO ligands (12 electrons) and a charge of 2– , a total of 14 electrons. If $x = 0$, the value of $4n + 2$ would be 18. Each Bi atom counts an additional 5 electrons, and each additional core atom increases $4n + 2$ by 4. At $\boldsymbol{x = 4}$, the total cluster valence electron count (34) equals $4n + 2$ (4 Bi atoms and 4 Ni atoms in core, so $n = 8$). Consequently, the formula is $[Bi_4Ni_4(CO)_6]^{2-}$.

15.28 $B_2H_6(Cp^*RuCO)_2$: Cp^*RuCO is a 15 electron fragment, 3 electrons short of 18. This fragment is isolobal to the 5-electron fragment BH_2, 3 short of 8 electrons. The metallaborane $B_2H_6(Cp^*RuCO)_2$ is therefore isolobal with B_4H_{10}.

$B_4H_{10} - 6H^+ \longrightarrow B_4H_4^{6-}$ (*arachno*)

(Continued on next page)

$B_3H_7(Cp^*RuH)_2$: Cp^*RuH is a 14 electron fragment, 4 electrons short of 18. This fragment is isolobal to the 4-electron fragment BH, 4 short of 8 electrons. The metallaborane $B_3H_7(Cp^*RuH)_2$ is therefore isolobal with B_5H_9.

$$B_5H_9 - 4H^+ \longrightarrow B_5H_5^{4-} \ (nido)$$

The reactions of $B_2H_6(Cp^*RuCO)_2$ with $Mn_2(CO)_{10}$ and $Re_2(CO)_{10}$, respectively, afford products with dramatically different structures. The $Mn_2(CO)_{10}$ reaction yields *arachno*$-[(Cp^*RuCO)_2B_3H_7]$ (left) and the novel bridged borylene complex $[\mu_3\text{-BH})(Cp^*RuCO)_2(\mu\text{-H})(\mu\text{-CO})\{Mn(CO)_3\}]$ (right, perspective from above the triply bridging borylene ligand).

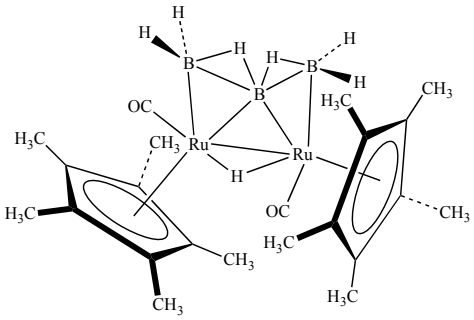

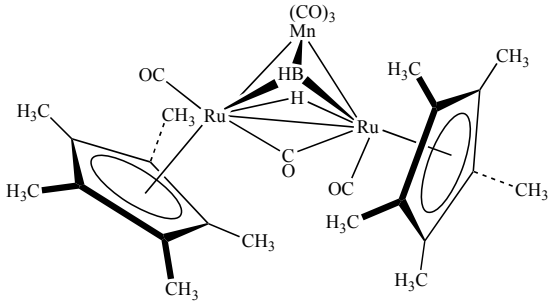

The reaction of $B_2H_6(Cp^*RuCO)_2$ and $Re_2(CO)_{10}$ provides $[Cp^*Ru(CO)(\mu\text{-H})]_2$ (below) as the only characterized product.

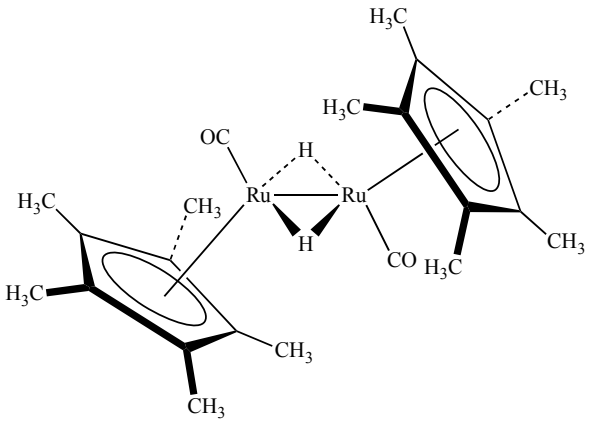

15.29 The cluster is below, with each Mo an abbreviation for $(\eta^5$-Cp*Mo$)$. The presence of molybdenum—molybdenum bonds is postulated to prevent BH capping of some of the cubane faces. The two boron atoms labeled as "1" are five-coordinate and are assigned a $^{11}B\{^1H\}$ NMR chemical shift of 131.5 ppm. The boron atoms labeled "2" are four-coordinate with bonds to three Mo atoms and one boron atom; the corresponding chemical shift for these two atoms is 94.4 ppm. The three boron atoms labeled "3" are four-coordinate with two bonds each to boron and molybdenum; the chemical shift for these three boron atoms is 58.8 ppm.

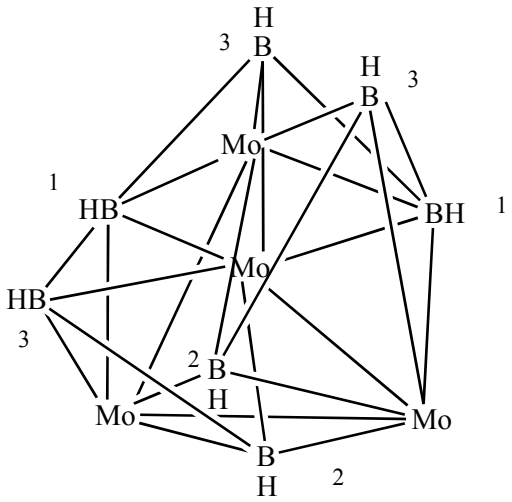

This cluster features four η^5-Cp* ligands, and pairs of these are chemically equivalent on the basis of the ^1H NMR spectrum. The "top" two Mo atoms feature bonds to five boron atoms and one Mo atom. The "bottom" two Mo atoms feature bonds to four boron atoms and two Mo atoms. These provide two unique chemical environments for the η^5-Cp* ligands.

15.30 Product yields for insertion of the dicarbollide cage into $[(\eta^6$-arene)Fe$][PF_6]_2$ were deemed lower with the pentamethylbenzene and hexamethylbenzene iron complexes as reactants (15-20%, compared to 48-70% with the less substituted benzenes) on the basis of stronger Fe—arene bonds with these more highly methylated cations. A variety of approaches were used to show correlations to the degree of methylation of the benzene. Figure 1 of the reference shows that the diamagnetic shielding of the CH cage hydrogen atoms increases with increasing number of arene methyl groups. The resonances for these CH hydrogen atoms shift upfield as the number of methyl substituents changes from 1 to 6. Similar linear correlations were observed between the ^{11}B chemical shift of the antipodal dicarbollide cage boron atom (labeled as 12 in Scheme 1) and the ^1H chemical shift of the hydrogen atom on this same boron atom; as the degree of methyl substitution increases at the arene ligand, these resonances progressively shift upfield. It is remarkable how sensitive the latter chemical shifts are to modulation of the donor ability of the arene ring since these atoms are separated from the iron atom by a relatively large number of bonds. The Fe^{2+}/Fe^{3+} redox potential decreases linearly as the number of methyl substituents increases; the complexes become progressively easier to oxidize (the complexes become better reducing agents) as the number of methyl groups increases.

15.31 **a.** Ge_9^{4-} has 40 valence electrons = $4n + 4$. Its classification is *nido*.

b. $InBi_3^{2-}$ has 3 + 3(5) + 2 = 20 valence electrons = $4n + 4$. Its classification is also *nido*.

c. Bi_8^{2+} has 8(5) – 2 = 38 valence electrons = $4n + 6$. It is an *arachno* cluster.

15.32 The reference notes that significant ion-pairing exists between the potassium ions and the highly negatively charged Zintl ions in K_3E_7 (E = P, As, Sb). Addition of cryptand[2.2.2] results in potassium ion complexation, attenuates the ion-pairing interaction, and renders the Zintl ions more effective nucleophiles. The IR spectroscopic data in the carbonyl region for $[K(2.2.2)]_3[E_7Cr(CO)_3]$ (below) indicate extensive π-backbonding in each case. On the basis of the lowest energy CO stretching frequency, one would tentatively rank the E_7^{3-} donor ability to the $Cr(CO)_3$ fragment as increasing as Sb < P < As, but these frequencies are sufficiently similar that it is difficult to clearly differentiate the donor ability of these Zintl ions.

Salt	IR ν(CO) (cm^{-1})
$[K(2.2.2)]_3[P_7Cr(CO)_3]$	1829, 1738, 1716
$[K(2.2.2)]_3[As_7Cr(CO)_3]$	1824, 1741, 1708
$[K(2.2.2)]_3[Sb_7Cr(CO)_3]$	1823, 1748, 1718

The electronic spectra of $[K(2.2.2)]_3[E_7Cr(CO)_3]$ are provided in Figure 5a of the reference. The tails of the absorptions assigned to intra-ligand E_7^{3-} charge transfer bands decrease in energy from PCr > AsCr > SbCr. Note that the λ_{max} of these charge transfer bands (Table 4) are nearly identical, although they do exhibit differences in their molar absorptivity constants, ε, in parentheses: PCr: 363 nm, (6600 $\frac{L}{mol \circ cm}$); AsCr: 365 nm, (11400 $\frac{L}{mol \circ cm}$); SbCr: 365 nm, (16000 $\frac{L}{mol \circ cm}$). The assignment of these intra-ligand charge transfer bands in $[K(2.2.2)]_3[E_7Cr(CO)_3]$ is reasonable since the identical trends are exhibited by the Zintl ions E_7^{3-} themselves; these absorptions are essentially unchanged upon coordination to the $Cr(CO)_3$ fragment.

A sketch of $[Cr(CO)_3(HSb_7)]^{2-}$ is below. The hydrogen ion binds to the Sb atom furthest from the Cr atom.

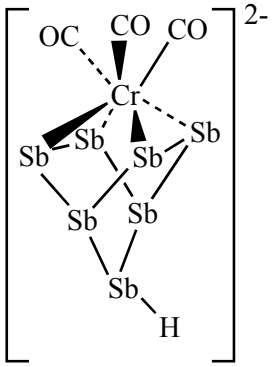

15.33 The Lewis structure of $[HP_7]^{2-}$ is below. It is interesting that this Zintl ion exhibits fluxional behavior in solution that renders all the phosphorus atoms equivalent on the NMR time scale.

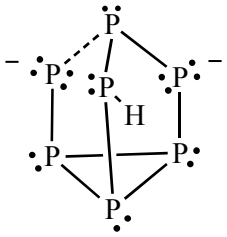

The most likely carbodiimide hydrophosphination mechanism is as follows, with nucleophilic attack at the carbodiimide carbon affording an intermediate amidinate that rapidly abstracts a proton from the Zintl ion cage. Evidence for intramolecular proton transfer is provided by isotopic labeling studies. When $[HP_7]^{2-}$ is used as a reactant towards carbodiimides in deuterated-solvents, the only amidine-functionalized products obtained feature N—H bonds. When the corresponding reactions with $[DP_7]^{2-}$ are conducted in protio-solvents, only amidine-functionalized products with N—D bonds are obtained. These experiments definitively prove the role of $[HP_7]^{2-}$ as the proton source, and strongly suggest the mechanism below.

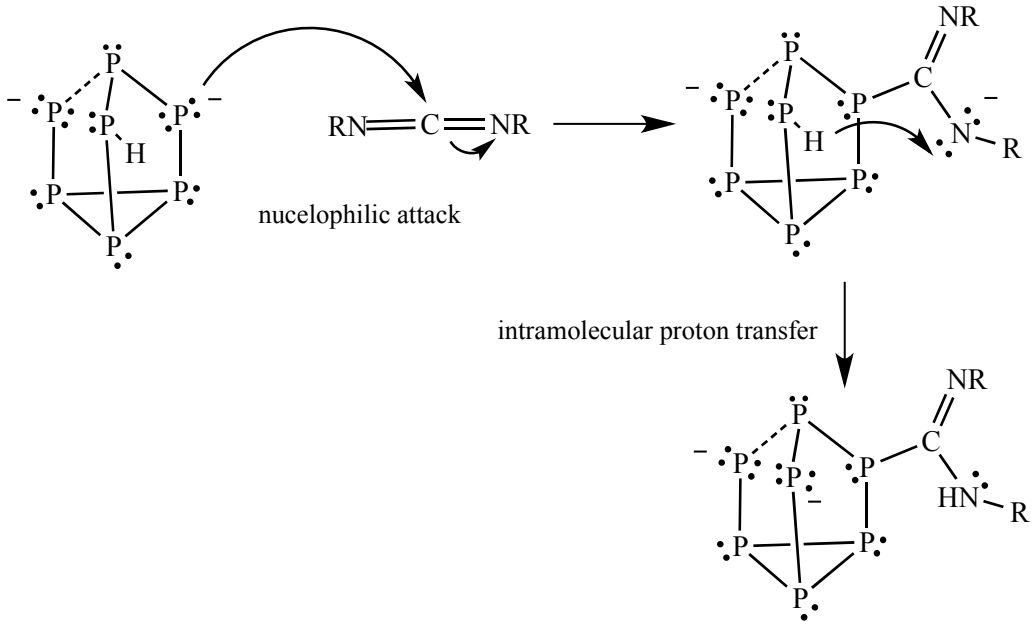

15.34 **a.** $m = 1$ (a single polyhedron)

$n = 5$ (each B atom counts)

$o = 0$ (no bridging atoms)

$p = 2$ (2 missing vertices)

8 skeletal electron pairs

b. $m = 2$ (2 polyhedra)

$n = 10$ (each B, C, and Co atom counts)

o = 1 (1 bridging atom, the cobalt)

p = 2 (2 missing vertices: the top part of the molecule is considered as a pentagonal bipyramid with the top vertex missing, and the bottom as an octahedron with the bottom vertex missing)

15 skeletal electron pairs

c. m = 2 (2 polyhedra)

n = 17 (each B, C, and Fe atom counts)

o = 1 (1 bridging atom, Fe)

p = 1 (1 missing vertex, the top atom of the incomplete pentagonal bipyramid)

21 skeletal electron pairs

15.35 **a.** C_{2v}

b. C_{5v}, D_{5h}

c. $[Re_2Cl_8]^{2-}$: D_{4h}; $[Os_2Cl_8]^{2-}$: D_{4d}

d. D_{2h}

e. C_{5v}

f. C_s, C_{2h}

g. Te_6^{2+}: D_{3h} Ge_9^{4-}: C_{4v}

15.36 **a.** T_d

b. I_h

15.37 **a.** The group orbitals are derived primarily from the 3*p* orbitals of phosphorus, which collectively resemble the five π orbitals for C_5H_5 in Figure 13.22. Diagrams of these orbitals can be found in the second reference. (See also Z-Z. Liu, W-Q. Tian, J-K. Feng, G. Zhang, and W-Q. Li, *J. Phys. Chem. A*, **2005**, *109*, 5645.)

Atomic orbitals on transition metals suitable for interaction (assuming metal centered below P_5 plane)

lowest energy group orbital: s, p_z, d_{z^2}
1-node degenerate pair: p_x, d_{xz}, p_y, d_{yz}
2-node degenerate pair: d_{xy}, $d_{x^2-y^2}$

b. The molecular orbitals of P_5^- are lower in energy than the similar orbitals of $C_5H_5^-$, giving rise to a generally stronger ability of P_5^- to π accept. For example, the energy match between 2-node orbitals and metal *d* orbitals may be closer in P_5^- complexes than in the case of ferrocene (Figure 13.28), enabling stronger interaction. An example of

such an interaction would be between an empty 2-node orbital of P_5^- and a $d_{x^2-y^2}$ orbital of a metal:

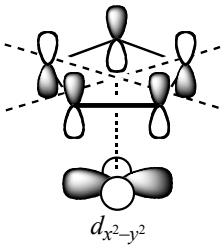

c. The reference provides an energy level diagram of the molecular orbitals of $[(\eta^5\text{-}C_5H_5)_2Ti]^{2-}$. In analyzing the orbitals it is important to see how the π orbitals of P_5^- ligands match up with *d* orbitals on Ti and how the resulting shapes illustrate how the lobes of these interacting orbitals merge (in the bonding orbitals) and how nodes are formed between them (in the antibonding orbitals).

15.38 The three types of interaction, σ, π, and δ, should be evident in the orbitals generated. In addition to the bonding interactions (see Figure 15.8) there should be matching antibonding interactions, with a nodal plane bisecting the metal–metal bond. The relative energies of the molecular orbitals should be similar to those on the right side of Figure 15.9, depending on the level of sophistication of the calculations used.

15.39 In addition to the σ, π, and δ interactions between *d* orbitals, shown in Figure 15.8, a σ interaction could occur between *s* orbitals of the two atoms:

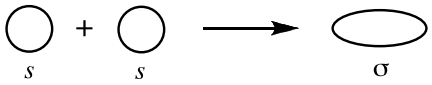

(In a chromium atom the valence 4*p* orbitals are empty, so interactions between them need not be considered.) The extent of the calculated interactions between the atomic orbitals is likely to differ significantly. Consequently, even though there may be six possible orbital interactions, the strength of such bonding is calculated to be significantly weaker than would be expected in a true "sextuple" bond. It is suggested that, for this exercise, the Cr–Cr distance be set at 166 pm, the equilibrium distance reported in the references.

15.40 **a.** The A_{1g} orbital should have a very large, nearly spherical lobe in the center of the cluster and six smaller, also nearly spherical lobes, on the outside of the borons (centered on the hydrogens).

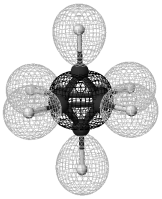

b. The T_{1u} orbitals should each have two regions where lobes of *p* orbitals on four B atoms merge, plus additional lobes, nearly spherical, centered on opposite hydrogens.

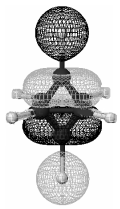

c. The T_{2g} orbitals should show how the lobes of adjacent *p* orbitals merge. The result should have four lobes, somewhat similar in appearance overall to a *d* orbital.

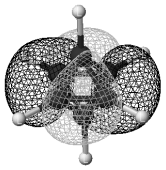

15.41 The orbitals are naturally much more complex, with 167 orbitals and 270 electrons. The T_{1u} and T_{2g} orbitals shown are from a Scigress Extended Hückel calculation.

a. The A_{1g} orbital should be similar to that for $B_6H_6^{2-}$ in Problem 15.31, with one large lobe in the center and smaller *d* orbital lobes on each of the Ru atoms. It is the HOMO, antibonding in symmetry, and the only orbital near this energy that involves carbon orbitals.

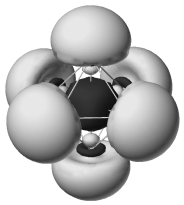

b. The T_{1u} orbitals should also be similar to the T_{1u} orbitals of $B_6H_6^{2-}$. There should be two large lobes, each derived primarily from *d* orbitals on four Ru atoms and a *p* orbital of the central carbon, plus lobes on opposite Ru atoms (the other Ru atoms). There may also be fragment lobes of *d* orbitals on the Ru atoms.

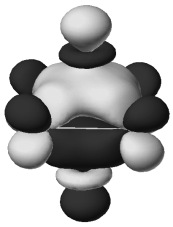

c. The T_{2g} orbitals are not directly involved in bonding with the carbon, but they do strengthen the cluster framework. The atomic orbitals should interact in sets of four, similarly to the T_{2g} orbitals in $B_6H_6^{2-}$, but some of the distinctive features of *d* orbitals should also be observable in the ruthenium cluster.

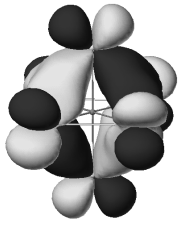

15.42 **a.** As in ferrocene, important interactions should be observed between 1-node group orbitals on the (in this case, Ge_5) ligands and d_{xz} and d_{yz} orbitals on cobalt (see example for ferrocene above Figure 13.27). With the Ge_5 ligands held in closer proximity by bonds between the top and bottom rings, interactions should also be found between 2-node group orbitals and the d_{xy} and d_{x2-y2} orbitals of Co and between 1-node group orbitals and p_x and p_y orbitals of Co.

b. In contrast to the cyclopentadienyl rings in ferrocene, primarily sigma bonding should be observed within the Ge_5 rings; the reported Ge–Ge distance in the rings is within the range of single bonds.

c. In addition to the comparisons mentioned above, it would be informative to see if in the $[CoGe_{10}]^{3-}$ cluster the interactions between the rings and the d_{z2} and p_z orbitals of Co are weak (because the lobes of these orbitals point toward the center of the rings) and to look for interactions involving the "doughnut" of the d_{z2}. If the software generates energies of the molecular orbitals, additional comparisons can be made between the energies of the cluster orbitals and those of ferrocene shown in Figure 13.28.